06

Study of products of hydrothermal treatment of oligochitosan solutions

© E.R. Gasilova,¶ A.O. Sitnikova, N.N. Saprykina, E.N. Vlasova, Yu.A. Skorik, A.V. Yakimansky

Branch of Petersburg Nuclear Physics Institute named by B.P.Konstantinov of National Research Centre „Kurchatov Institute“ — Institute of Macromolecular Compounds,
199004 St.-Petersburg, Russia
¶ e-mail: Katja.Gasilova@gmail.com

Received October 18, 2024
Revised October 18, 2024
Accepted October 2024, 2024

Porous carbon spheres of tens to thousand nanometers size and luminescent carbon nanodots of less than 10 nanometer size can be formed via a hydrothermal treatment of polysaccharides. Both types of carbon structures have a wide range of applications. However, the phase separation between carbon nanodots and carbon spheres during the hydrothermal treatment was not studied. In the current work, both phases formed by hydrodynamic treatment of dilute aqueous dispersions of oligochitosan were studied. The luminescence and UV/vis absorption of carbon nanodots were examined; the carbon spheres were characterized by light scattering and scanning electron microscopy. Upon increasing the duration of hydrothermal treatment, the carbonization degree of both components and the size of carbon spheres increased. For the first time, the luminescence of carbon nanodots originating from oligochitosan was shown to depend on the autoclave filling.

Keywords: carbon nanodots, carbon spheres, hydrothermal synthesis, light scattering, luminescence, scanning electron microscopy.

DOI: 10.61011/TP.2025.02.60832.232-24

Introduction

Focus has been made on hydrothermal treatment of organic solutions as a cheap organic waste recycling technique due to the growing environmental issues. Several reactions take place during the hydrothermal treatment, including hydrolysis, isomerization, dehydration, condensation polymerization and aromatization [1]. Spherical porous carbon particles from 50 nm to several micrometers in size, so-called carbon spheres (CS), that result from carbonization, are also of interest. CS have prospects of application in various fields (as supercapacitors, in catalysis and biomedicine) [2]. Moreover, hydrothermal treatment of organic solutions may also give luminescent nanoparticles smaller than 20 nm, so-called carbon nanodots (CND). CND is a new class of luminescent nanoscale structures discovered in 2004 during the analysis of carbon nanotube synthesis products [3]. CND contain mutually ordered inclusions of conjugated aromatic $-C=C$ domains dispersed in an amorphous carbon matrix. CND surface contains various groups ($-C=O$, $-COOH$, $-NH_2$, $-OH$, etc.). Charged surface groups are responsible for the stability of C dot dispersions in water. Advantage of CND for biomedicine applications compared with semiconductor and perovskite quantum dots and with organic dyes is in CND non-toxicity, higher stability and dispersibility in water [4]. Explosive development of luminescent property studies and CND preparation techniques was caused by a wide prospect of application — in biomedicine, photocatalysis and photovoltaics. The presence of dopant atoms (nitrogen, sulfur, phosphorus and boron) in precursors leads to the inclusion of these atoms into CND and the variation of their luminescence spectra. Nucleation and growth of nuclei of ordered CND cluster during processing of precursor solutions are the least understood [5], and the division of a reaction medium into CND and CS hasn't been studied, in fact. Optical properties of CND are quite difficult for interpreting due to a complex CND structure that includes various functional surface groups, carbon atoms with sp^2- and sp^3-hybridization, inclusions of locally ordered aromatic carbon spots in the amorphous matrix. A wide variety of CND produced from various molecules and macromolecules using various techniques has been accumulated by now. CND luminescence is treated in a similar manner to quantum dots that depend on quantum-size effects or in a similar manner to luminescent properties of graphenes, which emission is caused by edge and inner states [6]. CND simulation by inclusion of aromatic compounds into a non-luminescent amorphous polymer matrix successfully reproduced the CND luminescence features [7]. Many researchers adhere to the Frenkel exciton model where the exciton emission is caused by electron–hole pair recombination on localized defects or surface states [8]. Some authors regard low-molecular aromatic compounds as the source of CND luminescence [9]. Since it is hard to compare the properties of CND prepared in several works using various synthesis conditions and precursors, studies investigating the influence of synthesis conditions on the luminescent properties of CND are of most interest. Similar fundamental research efforts were taken for CND made from concentrated solutions of low-molecular compounds. For example, the following effects were studied for hy-

drothermal CND: the influence of autoclave filling volume (ΔV) on the sizes of CND made from sucrose solutions [10]; the influence of hydrothermal treatment time (Δt) on the luminescent properties of CND made from dextrose in water solutions [11]; the influence of reaction temperature (T) on the quantum yield of CND made from solutions of citric acid and urea (as a nitrogen source) [12]. However, note that, after CND synthesis from concentrated low-molecular solutions, most of the newly formed compounds precipitate.

CND made by means of hydrothermal treatment of natural polysaccharide solutions are of principal practical interest due to the environmental friendliness of hydrothermal synthesis and cheap raw materials. Nitrogen-containing natural compounds, with chitosan being the best known among them, are the promising raw materials for making CND with the highest quantum yield [13,14].

The objective of this work was to study the influence of hydrothermal synthesis conditions (duration, temperature and autoclave filling degree) of chitosan solutions in water on the luminescent properties of CND. Since oligomers, unlike high-molecular chitosans, can be dispersed even in water [15], hydrothermal synthesis of chitosan oligomer (OCS) solutions in water was performed to prepare CND and CS. OCS solutions in water appeared to be not molecularly dispersed, as they contained submicron colloidal particles. Since the local concentration of OCS in initial submicron particles was high, hydrothermal synthesis of CND was performed with the concentrations of precursor lower by one to two orders of magnitude than in most studies of hydrothermal synthesis of low-molecular compounds. A precipitate was almost absent, whereas the dispersions contained two fractions — luminescent CND and large CS whose size was analyzed by light scattering in the solution and by scanning electron microscopy in dried state. The task consisted in investigating the influence of synthesis conditions (duration Δt, temperature T and autoclave filling volume ΔV) of OCS aqueous dispersions on the properties of both fractions (CND and CS). IR spectra were used to analyze the chemical structure variation due to hydrothermal treatment.

1. Experimental procedure

Chitosan oligomer (Bioprogress, Russia) (molecular weight $1.5 \cdot 10^4$, deacetylation degree 97%) was used [16]. Dilute solutions (concentration $c = 0.5$ mg/ml) were treated by hydrothermal synthesis in a 50 mL teflon-lined autoclave. The synthetic parameters are given in the table. The synthetic conditions will be hereinafter designated as: $T/\Delta t/\Delta V$ (T — synthesis temperature, Δt — synthesis duration, ΔV — oligochitosan solution volume in the autoclave).

Dynamic (DLS) and static (SLS) light scattering of initial OCS dispersions and hydrothermal synthesis products were measured using a Fotocor_FC system. A 20 mW helium-neon laser ($\lambda = 632.8$ nm) was used as a light source. Decalin bath temperature was 25 ± 0.1°C. The scattering angle θ was varied automatically from 40 to 130° and than back to 40° in 10° steps. At each scattering angle, the signal was integrated during 80 s. Autocorrelation functions (ACF) of light scattering intensity were analyzed by using DynaLS program allowing to determine the hydrodynamic equivalent sphere radius R_h calculated using the Stokes–Einstein equation on the assumption that particles have a form of spheres. Apparent hydrodynamic radius was determined at each angle$R_h(\theta) = kT/(6\pi\eta_s D)$, where k — is Boltzmann's constant, η_s — is the solvent viscosity, D — is the mutual diffusion coefficient determined by the ACF decay rate: $D = \langle\Gamma\rangle/q^2$, where $q = 4\pi n \sin(\theta/2)/\lambda$ — is the wave vector, (n — is the refractive index of a solvent), $\langle\Gamma\rangle$ — is the ACF decay rate. R_h was determined by extrapolating $R_h(\theta)$ to $\theta \to 0$.

Radius of gyration $R_g = (\langle R_g^2\rangle)^{1/2}$ was calculated using the Berry equation [17] describing the angular dependence of excess scattered light intensity equal to the solution scattering intensity (I) minus the solvent scattering intensity (I_s):

$$\frac{1}{\sqrt{P(\theta)}} = 1 + q^2\langle R_g^2\rangle/6, \qquad (1)$$

where $\langle R_g^2\rangle$ is the rms radius of gyration, $P(\theta) = [I(\theta) - I_s(\theta)]/[I(0) - I_s(0)]$ — is the form factor.

Electrostatic potential was determined using the Fotocor-kompakt-Z electrophoretic DLS (EDLS) system (25 mW 638 nm laser). Electrophoretic mobility under applied electric field is defined as $\mu_E = v/E$, where v is the velocity measured by the EDLS method. Electrostatic surface potential (ξ) was determined using the Smoluchowski equation $\mu_E = \varepsilon\varepsilon_0\xi/\eta_s$, where ε and ε_0 are solution and vacuum permittivities, respectively.

Hydrothermal treatment conditions for oligochitosan solutions in water

T, °C	Δt, h	ΔV, ml	QY, %
On the treatment durationΔt			
180	6	20	3.4
180	16	20	3.4
180	18	20	9.0
180	24	20	9.3
On autoclave filling volume ΔV			
180	24	5	1.8
180	24	16	5.2
180	24	35	6.6

Note. QY — luminescence quantum yield.

Absorption spectra were measured using a UV-1600 and UV-1800 (Shimadzu) instruments. Fluorescence spectra were measured on a RF-3600 and RF-5301 (Shimadzu) with xenon lamps as light sources. For dispersion luminescence measurement, CND were diluted 10 fold and filtered through nylon syringe membrane filters of 0.1 and 0.22 μm pore sizes. Dialysis of the dispersions was carried out through dialysis membranes with $\leq$ 1000 Da cut off.

Luminescence quantum yield (QY) was calculated as follows

$$\mathrm{QY} = 0.54\,\frac{L_x}{A_x}\,\frac{A_{st}}{L_{st}}\,\frac{n_x^2}{n_{st}^2}, \qquad (2)$$

where 0.54 is the luminescence quantum yield of quinine sulfate in 0.1 N H_2SO_4; A is the absorption amplitude at the excitation wavelength; L is the integral under the luminescence maximum in the overlap of the standard and test substance spectra. Indices st and x refer to the quinine sulfate fluorescent reference standard and test solution, respectively.

IR spectra were measured using a Vertex-70 (Bruker) spectrometer equipped by replaceable Zn−Se crystal with fixed reflection angle (PIKE Technologies).

Scanning electron microscopy (SEM) was performed on a Jeol GSM-35CF microscope. A voltage of 5 kV was used, detector SE2. The dilute dialyzed water solutions of initial OCS and OCS dispersions prepared by means of hydrothermal synthesis were dried on an aluminum substrate at room temperature.

2. Results

2.1. Evaluation of oligochitosan nanoparticle sizes

Figure 1 shows a microphotograph of dried OCS samples made by the electron microscopy method.

OCS forms spherical nanoparticles with a mean diameter of 90 nm, whose morphology resembles spherulites. Static and dynamic light scattering methods were used to determine the radius of gyration and hydrodynamic radius of OCS in water solutions $R_g \approx 200$ nm, $R_h = 159$ nm (solutions were centrifugated during 10 min at 8000 rpm). The difference in spherical nanoparticle sizes between the solution and solid state is indicative of considerable swelling of OCS particles in the solution. ξ potential of OCS in water solution was positive ξ=23 mV indicating that positively charged NH_3^+ groups were present on the nanoparticle surface [18].

2.2. Bimodal size distribution of hydrothermal synthesis products

Light scattering of unfiltered samples was caused by submicron colloids whose size increased with the duration of synthesis (Figure 2, a).

Proximity of the magnitudes of R_g and R_h is indicative of a spherical shape of submicron particles. Submicron

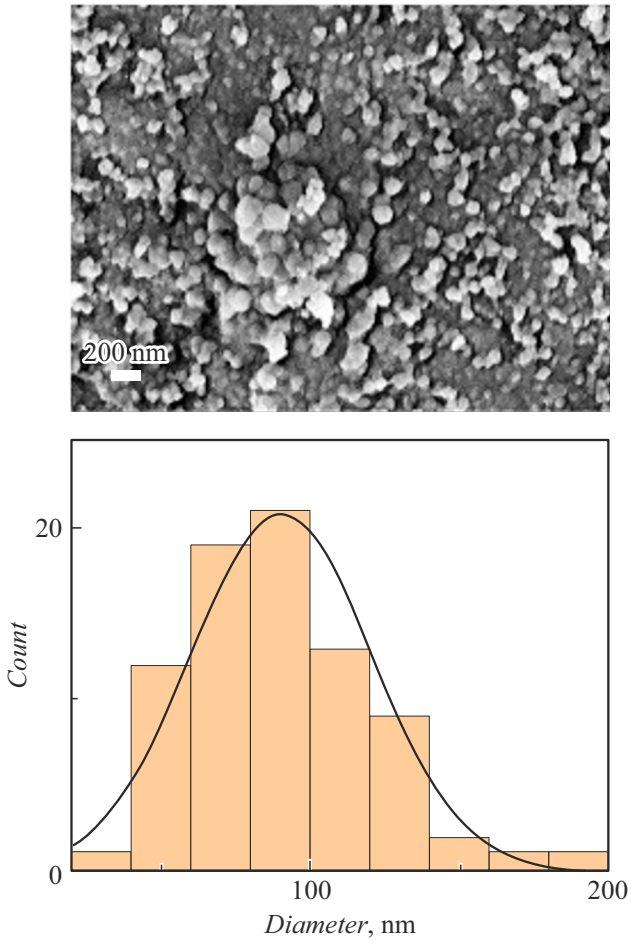

Figure 1. SEM microphotograph of OCS particles, (scale 200 nm) and diameter distribution histogram.

particles are nanogels as it follows from comparison of the angular dependence of scattered light intensity in the Kratky coordinates (Figure 2, b) with analytical curves calculated for the form factor of linear polymers (C=1) and nanogels (C=0) [19]:

$$P(q) = \frac{1 + Cu^2/3}{\left(1 + \frac{(1+C)u^2}{6}\right)^2}. \qquad (3)$$

Submicron nanogels were removed effectively by filtration through filters with 0.1 and 0.22 μm pore size as shown by dramatic decrease in the scattering intensity to the level that was 3−4 times as high as that of the solvent (water). R_h of the fine fraction was not evaluated because it was lower than 2 nm, however, the fine fraction made a considerable contribution to the luminescence (Figure 3, a). After dialysis through 1000 Da pores, the submicron nanogels remained in the solution (according to the light scattering data), however, their luminescence was low (Figure 3, a). Luminescent particles remained in the solution after filtration.

Figure 3, b demonstrates typical absorption spectra of initial, dialyzed and filtered dispersion 180/6/20. The absorption spectra of unfiltered initial dispersion has a shoulder

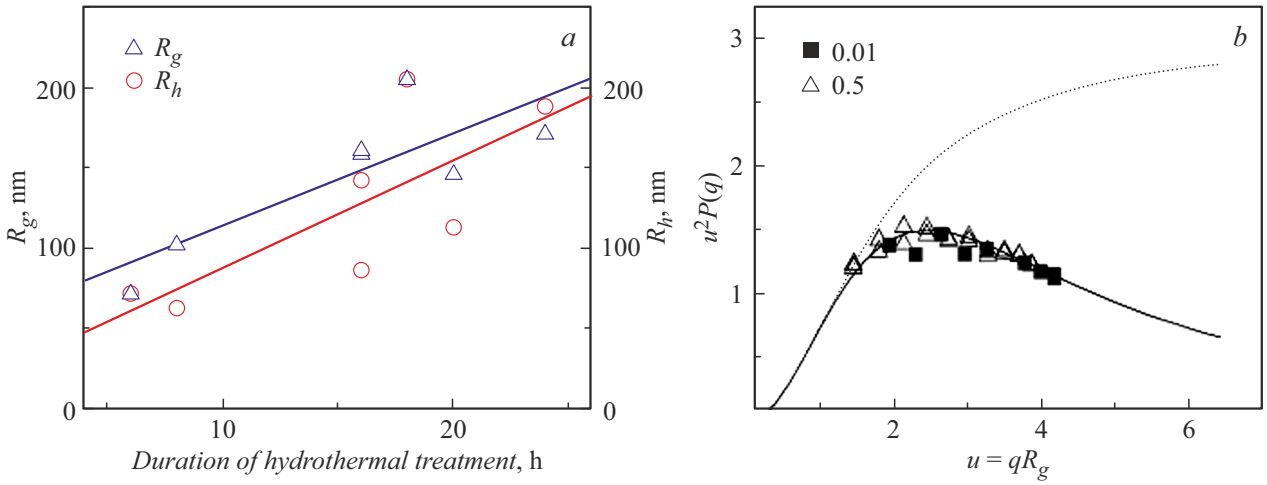

Figure 2. *a* — dependence of submicron particle sizes in dispersions obtained by hydrothermal synthesis of OCS solutions on Δt for series 180/Δt/20; *b* — dimensionless angular dependence of the reduced form factor on the reduced radius of gyration for dispersion 180/16/20. The dashed line was calculated using equation (3) for linear macromolecules, the solid line was calculated for nanogels. Dots correspond to the concentration values given in g/l.

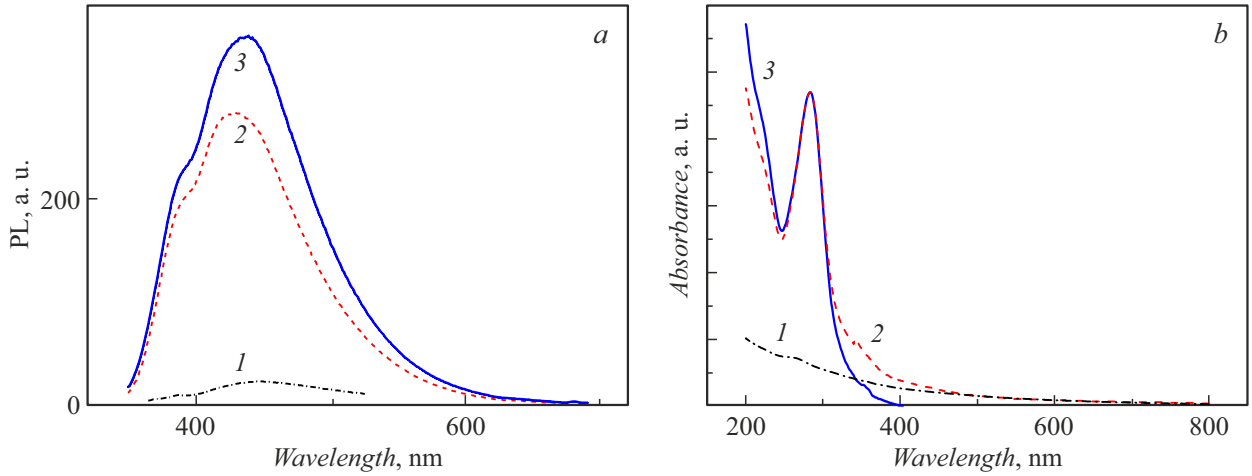

Figure 3. Luminescence (*a*) and absorption (*b*) spectra of dispersion 180/6/20. Designation of curves: dialyzed (*1*), initial (*2*) and filtered (*3*). Excitation wavelength is 340 nm. Absorption spectra of the initial and filtered solutions are normalized to the maximum amplitude. Absorption spectrum of the dialyzed solution coincides with tail of initial dispersion spectrum.

at 200 nm assigned to sp^2-hybridization of −C=C− atoms, and an absorption maximum at 280 nm caused by sp^3-hybridization of C−O, C−N bonds [18].

Moreover, a low-intensity absorption tail, that declines monotonously to the visible region, is observed. For the dialyzed sample, mainly a declining part can be seen that is indicative of a contribution to scattering from submicron spheres to extinction spectra. During filtration, submicron nanogels were removed and, consequently, the tail responsible for their contribution to extinction disappeared. The remaining absorption tail is likely associated with surface groups or CND defects, while the short-wavelength shoulder and absorption maximum should be assigned to conjugate aromatic fragments in the CND core. Note that this picture is typical of most CND absorption spectra, and the maximum luminescence of CND is excited exactly in the absorption tail region.

Thus, hydrothermal treatment of dilute OCS solutions gave rise to phase separation into non-luminescent spherical submicron colloidal nanogels (CS) and low-molecular luminescent phase of CND.

2.3. Microphotographs of dried dialyzed CND dispersions

Figure 4 shows microphotographs of dialyzed dried dispersions 180/6/20 (left) and 180/16/20 (right).

After the 6-hour synthesis, linear fragments of oligomer molecules probably remained and formed needle shaped-crystals. Moreover, there are spherical CS (with a mean

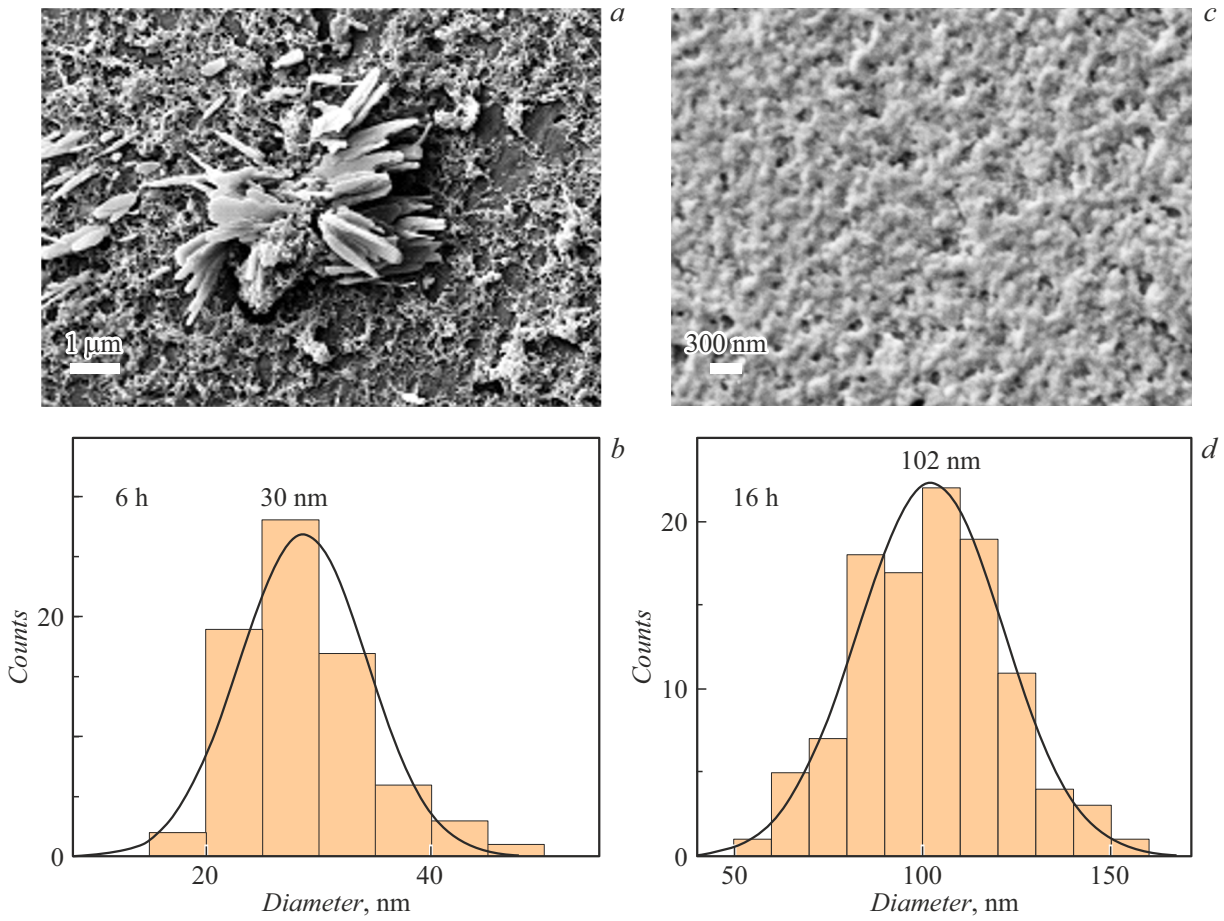

Figure 4. SEM microphotographs of dried dialyzed dispersions: 180/6/20 (scale 1μm) (*a*) and 180/16/20 (scale 300 nm) (*c*). CS diameter histograms 180/6/20 (*b*) and 180/16/20 (*d*).

diameter of 30 nm) embedded into the amorphous gel-like matrix. After the 16-hour synthesis, linear fragments disappeared, CS size grew to 100 nm, they were still embedded into a gel-like amorphous matrix. Thus, the size of dried CS increases with the growth of Δt similar to the growth of CS colloidal sizes. The CS size decreases considerably during drying compared with the size of swollen colloidal spherical gels. The amorphous portion that is self-organized during drying on substrate is apparently assigned to low-molecular fragments whose molecular weight exceeded the dialysis membrane pore size (1000 Da).

2.4. IR spectra of oligochitosan before and after hydrothermal treatment

IR spectra before and after hydrothermal treatment are shown in Figure 5. As a result of hydrothermal treatment, bands 3120, 3040 cm^{-1} appear in the spectrum and may be assigned to vibrations of various compounds containing $CR^1R^2{=}CHR^3$ groups. Band 1402 cm^{-1} in hydrothermally treated samples may be associated with tertiary alcohols. Band 1615 cm^{-1} induced by the hydrothermal treatment indicates that C=C bonds have been formed. Band

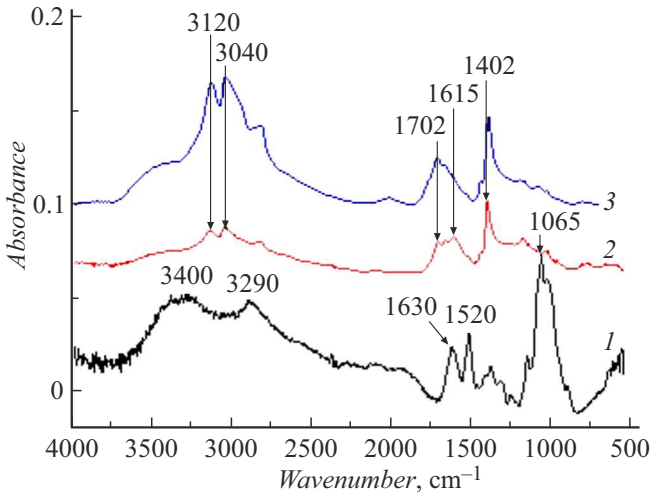

Figure 5. IR spectra of the initial OCS (№1) and lyophilized dispersions 180/6/20 (№2) and 180/16/20 (№3).

1702 cm^{-1} in the hydrothermally treated samples indicates that vibrations of C=O groups of carboxylic acids have occurred. Formation of $-COO^-$ groups during the CND

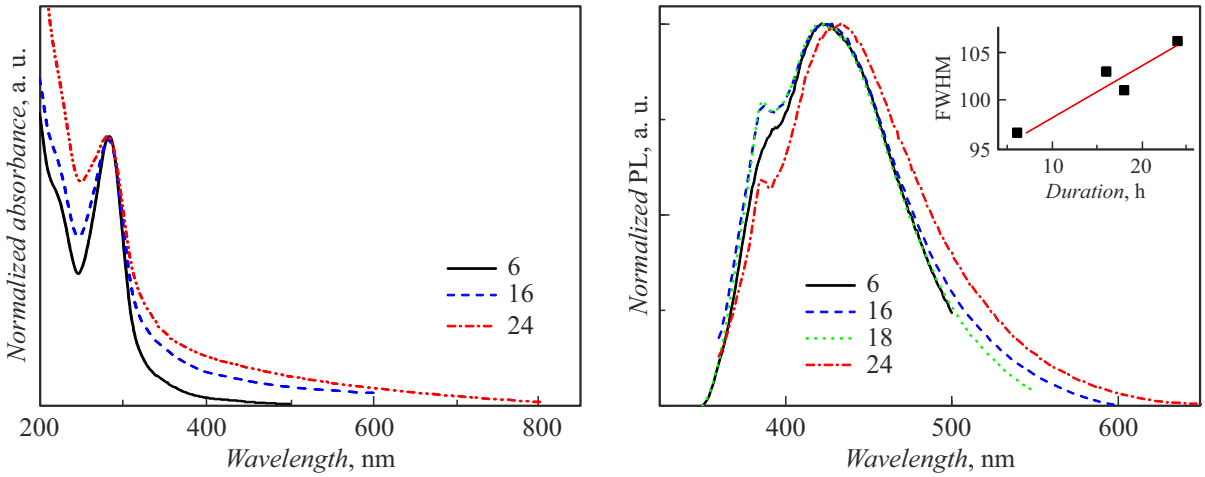

Figure 6. Influence of the synthesis duration on the absorption spectra (left) and FWHM luminescence line width (right) of CND series_180/Δt/20. The inset shows the dependence of the FWHM line width on the synthesis duration. The curves are designated by the synthesis duration in hours. CND dispersions are 10-fold diluted.

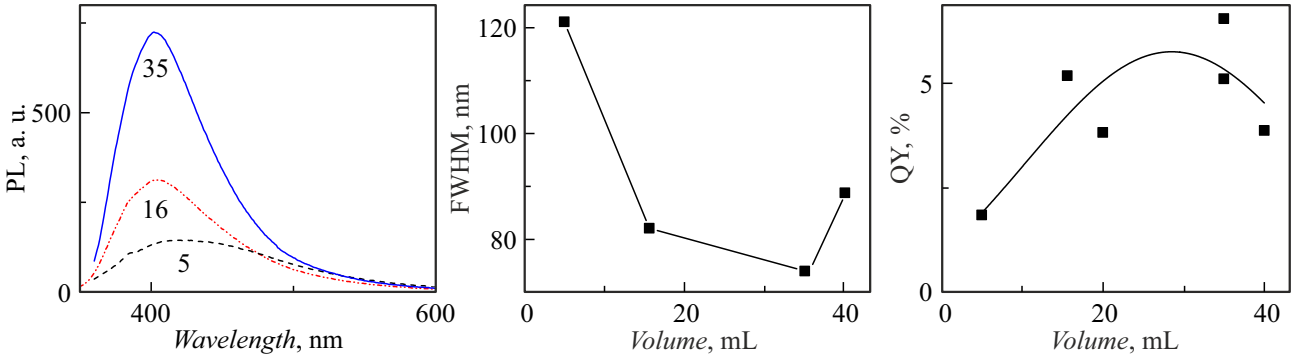

Figure 7. Luminescence spectra of CND series_180/24/ΔV normalized to A_x (the amplitude of absorption spectra at the excitation wavelength) (left); dependences of FWHM (center) and QY (right) on ΔV. The curves are designated by the autoclave filling volume in milliliters

synthesis is also demonstrated by the change of sign of ξ-potential from plus for OCS solutions (+20 mV) to minus (−9 mV) for sample 180/6/20. As Δt increases, the intensity of band 1702 cm^{-1} grows indicating that the content of acid residues increases. Further disruption of glycosidic bonds takes place simultaneously which is demonstrated by the decrease in the absorption intensity at 1100−1000 cm^{-1}. Instead of the band of OH groups of OCS (3400 cm^{-1}), bands 3120, 3040 cm^{-1} arise. They may be assigned to emerging stronger hydrogen bonds of acid groups.

2.5. Influence of the hydrothermal synthesis time on the absorption spectra of hydrothermal synthesis products

Figure 6 shows the absorption spectra of unfiltered hydrothermal synthesis products (series 180/Δt/20 at Δt = 6h, 16 h and 24 h). All spectra are characterized by a shoulder at $\sim$ 220 nm (sp^2-hybridization), maximum at $\sim$ 280 nm (sp^3-hybridization) and a slowly declining low-intensity absorption tail that extends up to the visible region. The spectra are normalized to the height of sp^3-maximum . It can be seen that the increase in Δt gives rise to a relative growth of absorption shoulder intensity, i.e. to the growth of double bond fraction. The declining absorption tails become longer and make a larger contribution to absorption with increasing Δt. It can be seen that the major luminescence maximum at $6 \le \Delta t \le 18$ is at 423 nm, and a bathochromic shift to 433 nm is observed only at the largest $\Delta t = 24$ h. At 200°C, the bathochromic shift is observed as early as at $\Delta t = 12$ h. All curves have an additional maximum at 386 nm. The FWHM line width grows with Δt.

2.6. Dependence of the luminescence on the autoclave filling volume and hydrothermal treatment time

Figure 7 (left) shows the dependences of luminescence spectra normalized to the absorption amplitude at the excitation wavelength on ΔV. It can be seen that the

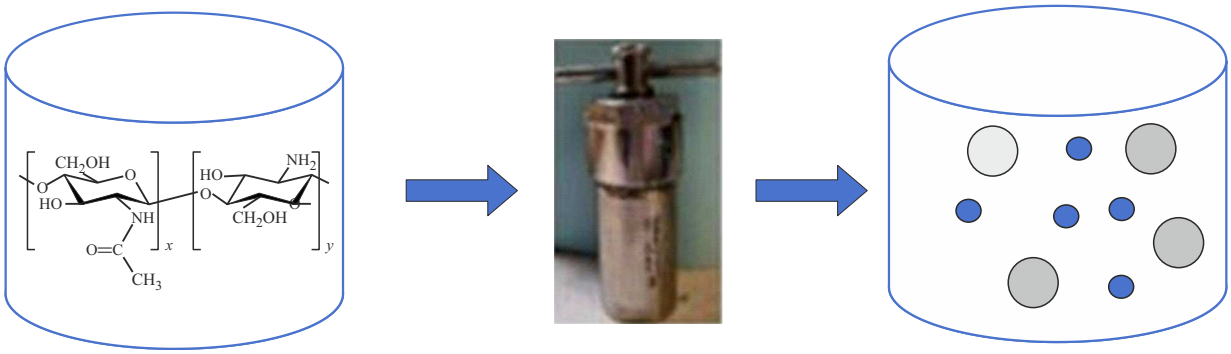

Figure 8. Synthesis scheme.

amplitude of PL/A_x spectra increases considerably with ΔV. Figure 7 (center) shows the dependences of the FWHM line width on ΔV. This dependence has the minimum.

Due to the fact that the dependences of the spectra amplitudes and FWHM on ΔV are mainly oppositely directed, the dependence of QY (absorption area) on ΔV is less pronounced. Nevertheless, the maximum QY corresponds approximately to a half-filled autoclave. The influence of Δt on QY may be estimated from the data listed in the table. At $T = 180°C$, QY grows with Δt, however, further carbonization with increasing temperature to 200°C reduces QY.

Conclusions

Initial dispersions of water-soluble chitosan oligomer and hydrothermal synthesis products were studied by the light scattering, scanning electron microscopy, and IR spectroscopy methods. Dependences of the luminescence and absorption spectra on the hydrothermal synthesis time and temperature and on the autoclave filling degree were examined. It is shown that dried solutions of the initial oligochitosan have a form of spherulites that swell considerably in water solutions. Dispersions prepared by means of hydrothermal synthesis of dilute oligochitosan solutions are two-phase (Figure 8).

The dispersions contain a fine luminescent CND fraction less than 2 nm in size and low-luminescent CS with submicron sizes. Analysis of angular dependences of light scattering shows that CS are nanogels. The luminescence quantum yield of fine fraction varies from 2% to 9% as the treatment time increases at 180°C. The minimum time (6-hour treatment) is insufficient for disruption of all glycosidic bonds in chitosan, and the remaining linear fragments of chitosan macromolecules are crystallized as shown in the SEM microphotographs. IR spectra also show incomplete destruction of the glycosidic bond absorption regions at the minimal treatment time $\Delta t = 6$ h. As the hydrothermal treatment time increases, further carbonization occurs, which is demonstrated by the growth of double bond contribution to the absorption spectra, and variations in the IR spectra. Using light scattering, it was established that the colloidal CS size grew with carbonization. Colloidal stability of CS is ensured by negative charges of carboxyl groups that were formed after chitosan hydrolysis. The CND quantum yield grows with the synthesis time from 6h to 24 h in series 180/Δt/20. Extreme behavior was first identified for the dependence of the CND luminescence on the degree of autoclave filling with chitosan solution. With the half-filled autoclave, the CND luminescence spectra width is minimal and the luminescence quantum yield is maximal.

Acknowledgments

The authors are grateful to D.N. Poshina and T.G. Tchulkova (Institute of Macromolecular Compounds, RAS) for their assistance.

Funding

The study was supported by grant of the Russian and St.-Petersburg's Science Foundations № 23-23-10005.

Conflict of interest

The authors declare no conflict of interest.

References

[1] M.H. Marzbali, S. Kundu, P. Halder, S. Patel, I.G. Hakeem, J. Paz-Ferreiro, S. Madapusi, A. Surapaneni, K. Shah. Chemosphere, **279**, 130557 (2021). DOI: 10.1016/j.chemosphere.2021.130557
[2] K.L.A. Cao, F. Iskandar, E. Tanabe, T. Ogi. KONA Powder Part. J., **2023**, 197 (2023). DOI: 10.14356/kona.2023016
[3] X. Xu, R. Ray, Y. Gu, H.J. Ploehn, L. Gearheart, K. Raker, W.A. Scrivens. J. Am. Chem. Soc., **126**, 12736 (2004). DOI: 10.1021/ja040082h
[4] B. Wang, S. Lu. Matter., **5**, 110 (2022). DOI: 10.1016/j.matt.2021.10.016
[5] C. Xia, S. Zhu, T. Feng, M. Yang, B. Yang. Adv. Sci., **6** (23), 1901316 (2019). DOI: 10.1002/advs.201901316
[6] C. Kang, S. Tao, F. Yang, B. Yang. Aggregate, **3**, 1 (2022). DOI: 10.1002/agt2.169

[7] M. Fu, F. Ehrat, Y. Wang, K.Z. Milowska, C. Reckmeier, A.L. Rogach, J.K. Stolarczyk A.S. Urban, J. Feldmann. Nano Lett., **15** (9), 6030 (2015). DOI: 10.1021/acs.nanolett.5b02215
[8] A. Demchenko. J. Carbon Res., **5**, 71 (2019). DOI: 10.3390/c5040071
[9] M. Righetto, F. Carraro, A. Privitera, G. Marafon, A. Moretto, C. Ferrante. J. Phys. Chem. C, **124**, 22314 (2020). DOI: 10.1021/acs.jpcc.0c06996
[10] N. Nammahachak, K.K. Aup-Ngoen, P. Asanithi, M. Horpratum, S. Chuangchote, S. Ratanaphan, W. Surareungchai. RSC Adv., **12**, 31729 (2022). DOI: 10.1039/d2ra05989d
[11] Z. Gan, X. Wu, Y. Hao. Cryst. Eng. Com., **16** (23), 4981 (2014). DOI: 10.1039/c4ce00200h
[12] Y. Zhang, Y. Wang, X. Feng, F. Zhang, Y. Yang, X. Liu. Appl. Surf. Sci., **387**, 1236 (2016). DOI: 10.1016/j.apsusc.2016.07.048
[13] H. Ababneh, B.H. Hameed. Int. J. Biol. Macromol., **186**, 314 (2021). DOI: 10.1016/j.ijbiomac.2021.06.161
[14] A.M. Villalba-Rodríguez, R.B. González-González, M. Martínez-Ruiz, E.A. Flores-Contreras, M.F. Cárdenas-Alcaide, H.M.N. Iqbal, R. Parra-Saldívar. Mar. Drugs., **20**, 1 (2022). DOI: 10.3390/md20120782
[15] M. Tian, H. Tan, H. Li, C. You. RSC Adv., **5**, 69445 (2015). DOI: 10.1039/c5ra08358c
[16] E.R. Gasilova, D.N. Poshina, A.O. Sitnikova, N.N. Saprykina, Y.A. Skorik. Chinese J. Polym. Sci. (English Ed.), **42**, 468 (2024). DOI: 10.1007/s10118-024-3069-9
[17] V.E. Eskin. *Rasseyanie sveta rastvorami polimerov* (Nauka, L., 1986) (in Russian)
[18] E.R. Gasilova, D.N. Poshina, A.O. Sitnikova, Y.A. Skorik. *Proceedings of International Conference on electrical engineering and photonics EExPolytech* (Saint Petersburg, Russia, 2023), p. 19–20. DOI: 10.1109/EExPolytech58658.2023.10318796
[19] W. Burchard. Macromolecules, **10**, 919 (1977). DOI: 10.1021/ma60059a008

Translated by E.Ilinskaya